IEEE Access
Multidisciplinary ⋮ Rapid Review ⋮ Open Access Journal

Received April 19, 2020, accepted April 30, 2020, date of publication May 7, 2020, date of current version May 20, 2020.

Digital Object Identifier 10.1109/ACCESS.2020.2992922

8 × 2-Element 60-GHz-Band Circularly Polarized Post-Wall Waveguide Slot Array Antenna Loaded With Dipoles

TAKASHI TOMURA, (Member, IEEE), YUTA SAITO, AND JIRO HIROKAWA, (Fellow, IEEE)
Department of Electrical and Electronic Engineering, Tokyo Institute of Technology, Tokyo 152-8552, Japan
Corresponding author: Takashi Tomura (tomura@ee.e.titech.ac.jp)

ABSTRACT In this paper, an 8 × 2-element 60-GHz band circularly polarized post-wall waveguide slot array antenna loaded with dipoles is proposed. The antenna is composed of a feeding circuit, radiating slots on radiating waveguides, and dipoles for polarization conversion. By integrating the feeding circuit and the radiating waveguides into a single dielectric layer, the total number of dielectric layers is reduced to two which greatly increases ease of mass production. The feeding circuit divides power into two and feeds the two radiating waveguides from their center. 8 × 2 radiating elements are composed of a slot and a dipole placed on the radiating waveguides. The elements are designed by standing-wave excitation. The antenna is fabricated by printed circuit board technology and its dimensions are 44.5 × 20.0 × 2.16 mm^3. The measured results show a 2.1-dB axial ratio, 15.6-dBi gain, and 57.2% efficiency at 61.5 GHz. The proposed antenna realizes a circular polarized array antenna with the minimum number of dielectric layers and electric performance comparable to conventional antennas.

INDEX TERMS Circular polarization, waveguide slot array antenna, post-wall waveguide, substrate integrated waveguide, 60-GHz band.

I. INTRODUCTION

The millimeter-wave band enables high data rate wireless communication because wider frequency bands are available than in the microwave bands [1]. The wireless communication is limited to line of sight because of low diffraction and high propagation losses. Many applications have been proposed for wireless communication between a base station and a user terminal or between user terminals [2], [3]. Antennas for base stations are required to be simple structures in terms of mechanical stability and productivity.

High gain antennas are used for base stations in the millimeter-wave band to compensate for the high propagation losses. Microstrip line patch array antennas are widely used for high gain planar antennas in the microwave band. However, they suffer from high transmission losses in the millimeter-wave band [4]. Post wall waveguides [5], also known as substrate integrated waveguides (SIW) [6], feeding circuits are widely used in the millimeter-wave band because of their low transmission losses [7].

The associate editor coordinating the review of this manuscript and approving it for publication was Davide Comite.

Circular polarization (CP) is adopted in antennas of base stations in order to reduce polarization mismatch between a base station and the user equipment [3]. A hollow waveguide fed circularly polarized slot array with printed dipoles [8], [9] or hexagonal apertures [10] offer low transmission losses but is not suitable for mass production. Low temperature co-fired ceramics (LTCC) based SIW CP array antennas realize wide bandwidths using 20 dielectric and 8 metal layers [11]. The measurement results are degraded because of fabrication tolerances, and the number of layers should be decreased as far as possible to reduce the complexity and fabrication costs. An ellipse-loaded circular slot array for the 60-GHz band realizes measured wideband and high-efficiency characteristics [12]. The slot array antenna [12] is fabricated by a printed circuit board (PCB) process and suitable for mass production. However, this antenna requires a reflector which makes the structure complex. A circularly polarized slotted SIW cavity antenna has a simple feeding circuit [13], [14] and 4 × 4 elements are placed on the cavity and fed by a single coaxial probe. However, it requires an air spacer between the slots and dipoles which weaken the physical strength and complicates production. Other shapes of polarization conversion

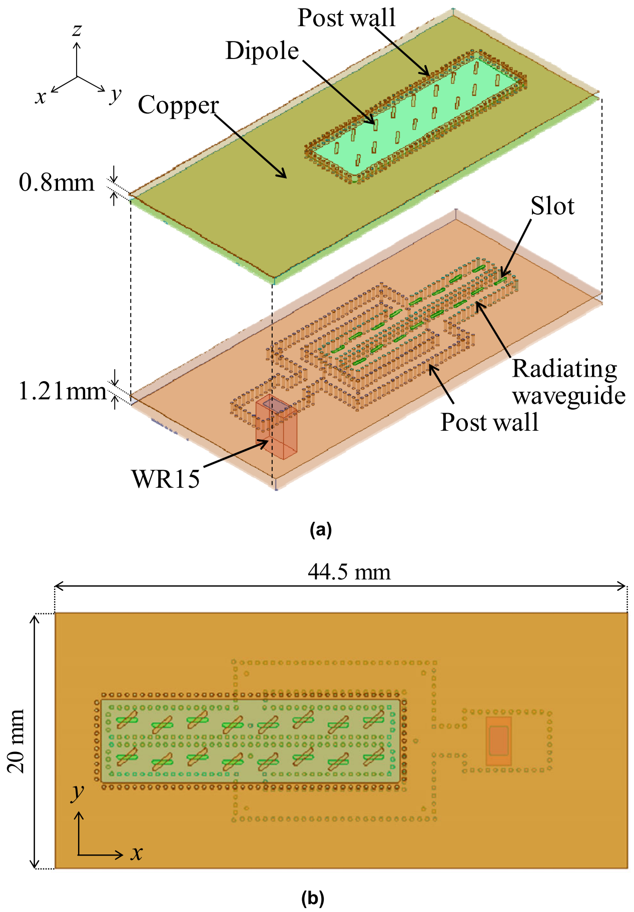

FIGURE 1. The antenna structure (a) exploded view, (b) top view.

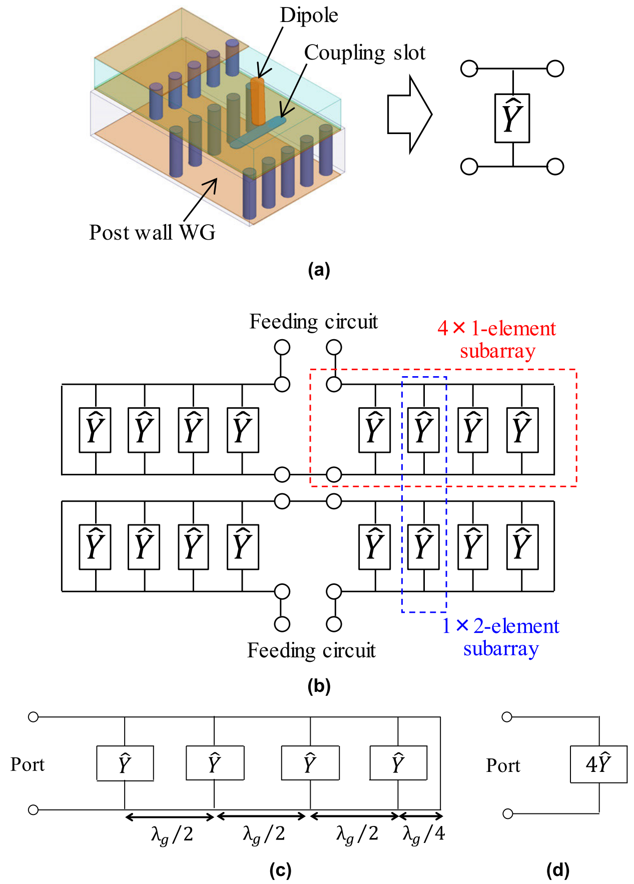

FIGURE 2. Equivalent circuits for (a) a single element, (b) an 8 × 2-element array, (c) & (d) 4 × 1-element subarrays.

elements have been investigated such as stacked curl [15], ME-dipole [16], [17], double spiral [18], helical [19], and dielectric resonator antennas [20]. However, they require more than three substrate layers.

In this paper, we propose a 60-GHz-band circular polarized array antenna with a much simpler structure than conventional ones [8]–[20] and which can be fabricated by conventional PCB technology. The antenna is composed of two dielectric layers and four metal layers. It does not require spacers or reflectors. The target bandwidth is channel two of IEEE 802.11ad [1], which is 59.5 - 61.5 GHz. The antenna is suitable for base stations and enables more practical mass production because of the simple structure and the fabrication by PCB technology. The design method and characterization of the fabricated antenna are detailed.

II. ANTENNA STRUCTURE

The antenna is composed of two copper-clad laminated substrates as shown in Fig. 1 (a). The substrate in the lower layer has a feeding circuit and radiating waveguides. The other substrate has dipoles. The substrates are made of poly tetra fluoro ethylene (PTFE) and have a 2.16 dielectric constant and 0.0005 loss tangent with 29-μm thick copper layer. The two substrates are bonded by a bonding film with dielectric constant, loss tangent, and thickness of 2.28, 0.003, and 67 μm, respectively.

The antenna is fed by a rectangular waveguide WR-15 from the back. The feeding circuit divides the power into two and feed the center of the radiating waveguides. Slots are placed on the broad wall of the radiating waveguide with constant spacing in the x-axis direction and excited with the same amplitude and phase. Dipoles are placed on each slot as shown in Fig. 1 (b) to change polarization from linear to circular. Around the dipoles there are post walls to prevent unwanted surface waves.

III. DESIGN

The radiation and the feeding part of the antenna are designed separately and then the designed parts are combined. The design frequency is 60.5 GHz and the target bandwidth is channel two of IEEE 802.11ad, 59.5 – 61.5 GHz [1].

A. RADIATION PART

First a desired admittance value of a single radiating element is determined and then the actual antenna dimensions are designed. Because a longitudinal slot on a waveguide is expressed by a shunt admittance element [21], the single radiating element is expressed by a single shunt admittance element as shown in Fig. 2 (a). The entire 8 × 2-element

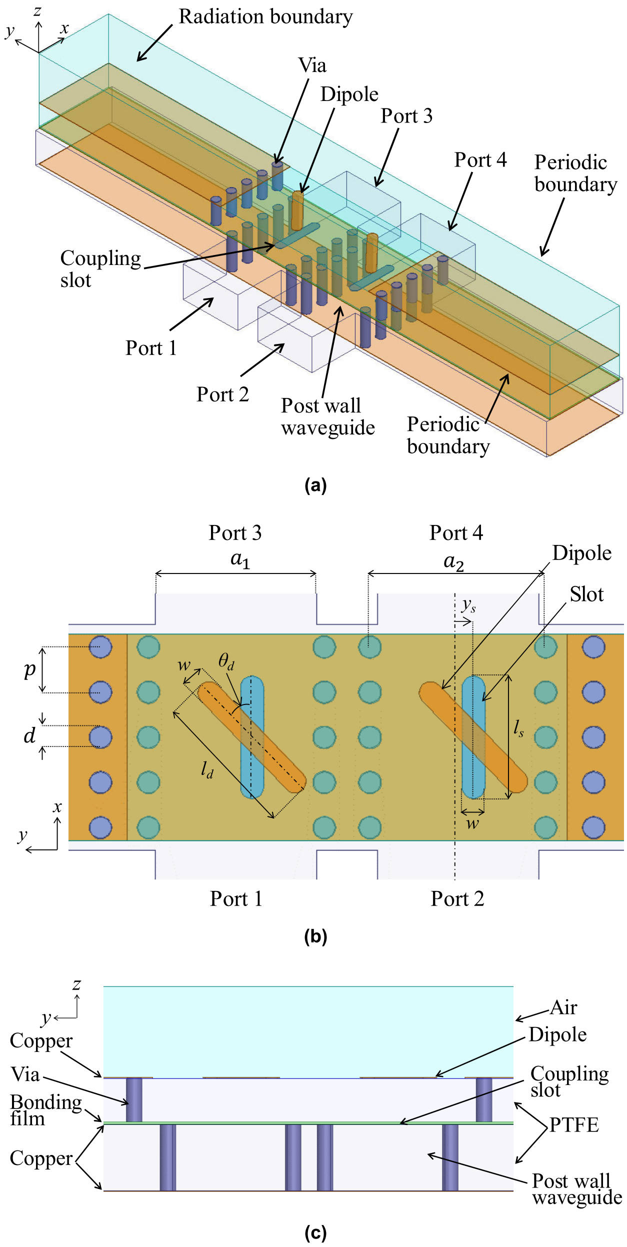

FIGURE 3. Analysis model for designing the radiating elements.

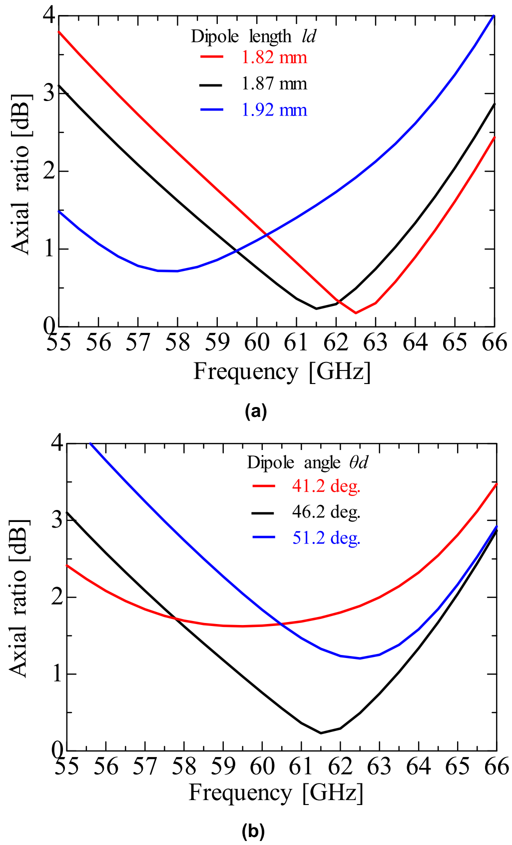

FIGURE 4. Frequency characteristics of the axial ratio by (a) the dipole length, (b) the dipole angle.

array is expressed by eight admittance elements as shown in Fig. 2 (b). The admittance value is determined for uniform excitation and matching. Because of the symmetricity of the structure, a quarter of the array, a 4 × 1-element subarray, is designed. The equivalent circuit of the four-element array is expressed by four cascaded shunt elements with normalized admittance $\hat{Y}$ and short termination as shown in Fig 2 (c). The array is designed by standing wave excitation [22], each element is placed with a constant spacing of half guided wavelength. To excite the elements uniformly, all of the admittance and the dimensions of the four elements are identical. Because the elements are placed with the half guided wavelength separation, the equivalent circuit can be simplified to a single shunt element of $4\hat{Y}$ as shown in Fig. 2 (d). The resulting desired admittance for the uniform excitation and matching is $\hat{Y} = 1/4$.

A 1×2-element subarray is used for designing the radiating element dimensions to include mutual coupling between the elements as shown in Fig. 3. The dipole and the slot are shifted from the center of the waveguide to control the radiation power. The dipole is rotated by θ_d from the waveguide axis to change the polarization from linear to circular. The width of the rectangular waveguide is determined so that the propagation constants of both the rectangular waveguide and post-wall waveguide are the same using the approximated equations [23], and the guided wavelength is 5.48 mm.

The design of the radiation part is as follows:

Step 1: Change the length and the angle of the dipole so that a low axial ratio is obtained. The frequency characteristics of the axial ratio can be controlled by the dimensions of the dipole as shown in Fig. 4

Step 2: Change the slot length to control the imaginary part of the normalized admittance as shown in Fig. 5 (a). The slot length affects both the real and imaginary part of the normalized admittance.

Step 3: Change the shift amount of the slot to change the real part of the normalized admittance as shown in Fig. 5 (b). The shift amount has the smaller effect on the imaginary part of the admittance.

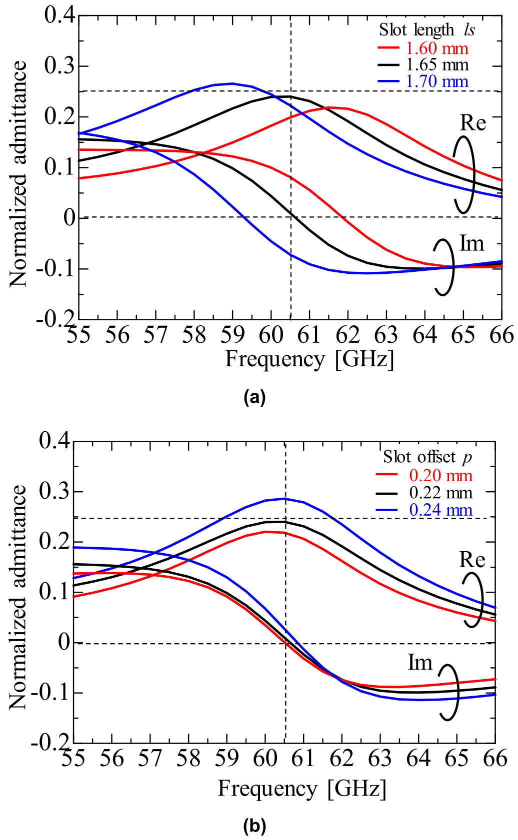

FIGURE 5. Frequency characteristics of the normalized admittance.

TABLE 1. Designed parameters of the radiating element.

Parameter	a_1	a_2	p	d	w
Value (mm)	2.31	2.12	0.6	0.3	0.3
Parameter	l_s	l_d	x_s	θ_d	
Value (mm)	1.87	1.65	0.22	46.2 deg.	

Step 4: Repeat steps 1 to 3 until a low axial ratio and desired normalized admittance are realized. The designed dimensions are shown in Table 1.

B. FEEDING PART

The feeding part consists of four components: a waveguide to the post-wall waveguide transition [24], a T-junction [25], an H-bend [26], and a τ-junction [27], [28] as shown in Fig. 6 (a). Each component is separately designed as shown in Fig. 6 (b) – (d) except for the waveguide to post-wall transition and the T-junction. The designed parameters and the reflections are shown in Table 2 and Fig 7, respectively. The reflection is below -10 dB over the target bandwidth.

C. FULL STRUCTURE

The designed radiation and feeding part are combined and the complete structure shown in Fig. 8 is analyzed. The designed reflection, gain, and axial ratio are shown in Figs. 9 – 11, respectively. The reflection is below -15 dB at the target frequencies. The gain is 16.9 dBi and the antenna efficiency is

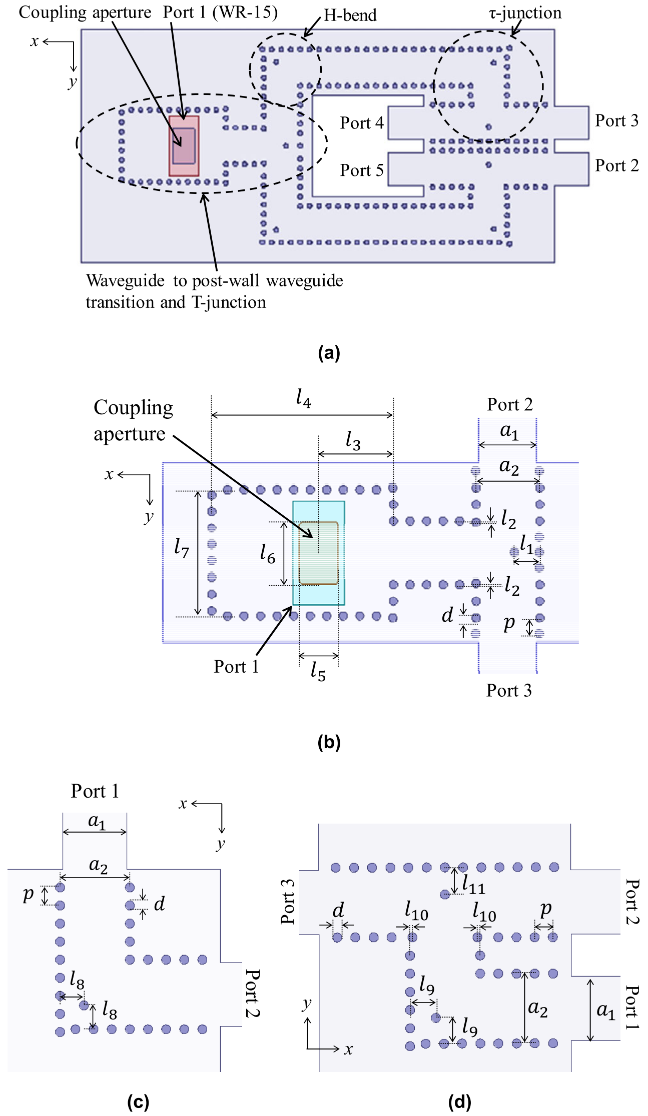

FIGURE 6. Analysis models for the feeding circuits.

TABLE 2. Designed parameters of the feeding circuit.

Parameter	l_1	l_2	l_3	l_4	l_5	l_6
Value (mm)	0.90	0.05	2.66	6.59	1.40	2.28
Parameter	l_7	l_8	l_9	l_{10}	l_{11}	
Value (mm)	4.57	0.79	0.85	0.06	0.90	

75.1% at 60.5 GHz with a 0.54-dB conductor loss and a 0.20-dB dielectric loss. The axial ratio is below 1.3 dB over the target bandwidth. The 1-dB gain down bandwidth is 5.6 GHz, which is wider than the two-channel bandwidth of the IEEE 802.11ad.

IV. MEASUREMENTS

The designed antenna was fabricated by PCB processes as shown in Fig. 12. The reflection and radiation characteristics of the fabricated antenna were characterized by a vector network analyzer and a near-field antenna measurement system in an anechoic chamber.

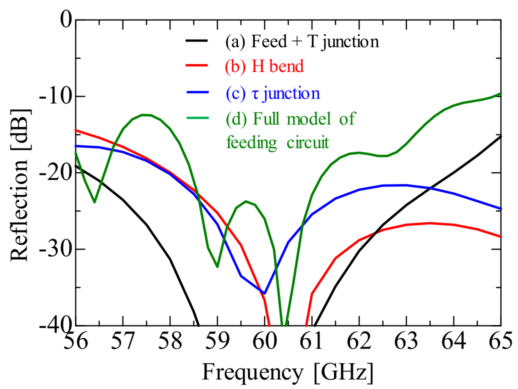

FIGURE 7. Frequency characteristics of the reflection of each component and the entire feeding circuit.

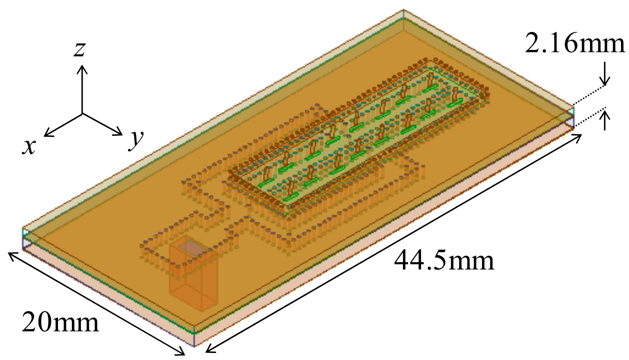

FIGURE 8. The analysis of the full structure.

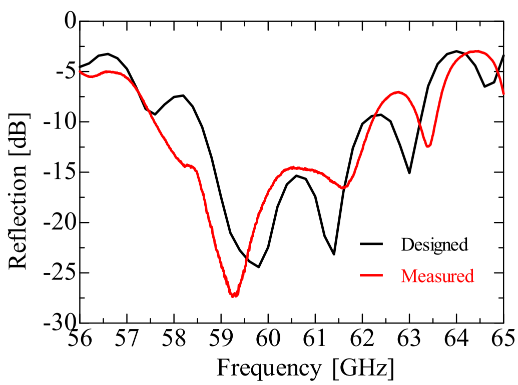

FIGURE 9. Frequency characteristics of the reflection.

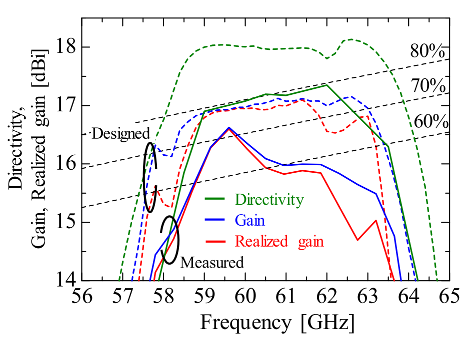

FIGURE 10. Frequency characteristics of the gain and realized gain.

The frequency characteristics of the measured reflection are similar to the simulated ones and below −14.5 dB over the target bandwidth as shown in Fig. 9. The measured frequency characteristics of the realized gain are better than 15.9 dBi in the target bandwidth as shown in Fig. 10. The difference between the realized gain and gain corresponds to the return loss [29] and the measured realized gain at 62.7 GHz is degraded because of the return loss. However, the measured frequency characteristics of the directivity is 1.0 dB lower than the simulation at the design frequency and the 1-dB down directivity bandwidth becomes narrower, from 9.2% to 7.7%. It is considered that the degradation of the directivity is a result of misalignment of the substrates in the y-direction. The simulated directivity and realized gain with misalignment of the dielectric for both the x- and y-directions is shown in Fig. 13 and Fig. 14, respectively. The x-direction misalignment has less of an effect on the directivity. However, the y-direction misalignment degrades the directivity more than that in the x-direction and a 150-μm misalignment decreases directivity by 1 dB below the designed value. The tendencies of the realized gain are similar to those of the directivity. The y-direction misalignment has a larger influence to the realized gain. The realized gain with a 100-μm misalignment shows similar characteristics to that of the measured realized gain.

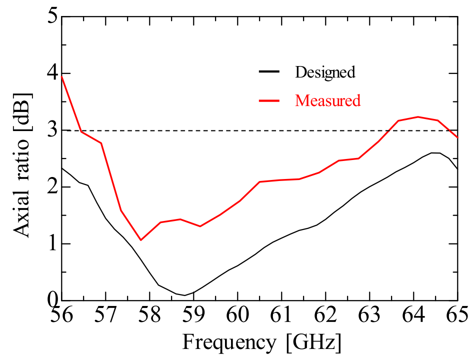

FIGURE 11. Frequency characteristics of the axial ratio.

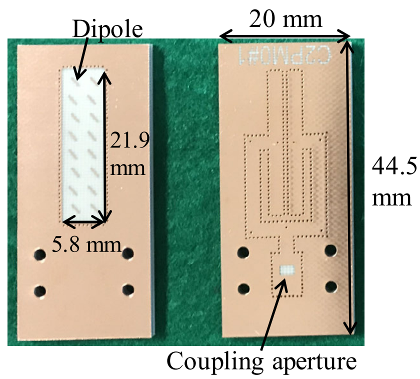

FIGURE 12. The fabricated antennas.

The frequency characteristics of the axial ratio were degraded by 1 dB at the design frequency and below 2.1 dB at the target bandwidth as shown in Fig. 11. The measured polarization mismatch is 0.3-dB higher than the designed polarization at the design frequency. The spinning linear patterns at 59.5, 60.5, and 61.5 GHz were measured as shown in Fig. 15 and higher sidelobe levels are observed at $\varphi = 0°$

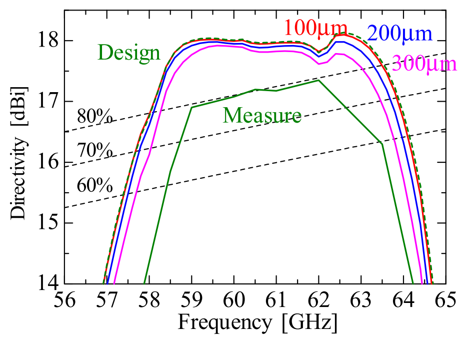

(a)

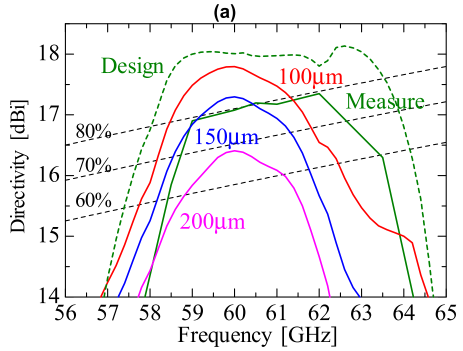

(b)

FIGURE 13. Simulated directivity with dielectric misalignment in (a) the x-direction and in (b) the y-direction.

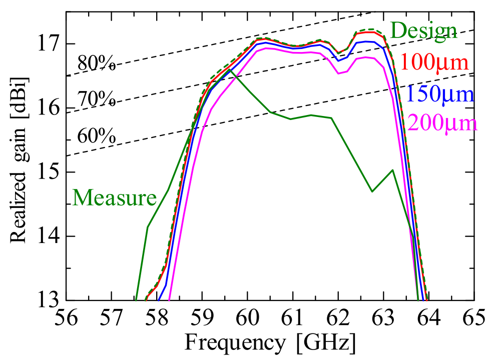

(a)

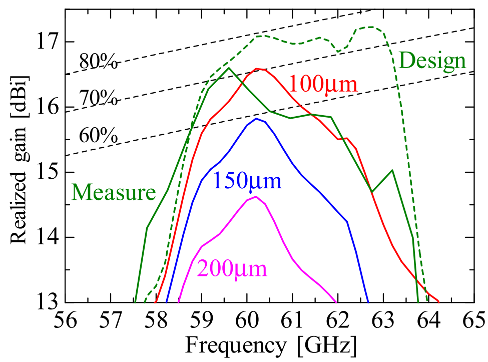

(b)

FIGURE 14. Simulated realized gain with dielectric misalignment in (a) the x-direction and in (b) the y-direction.

because of the fabrication tolerance. The oscillation of the measured radiation patterns results from the spinning linear measurement method [30] and its amplitude corresponds to the axial ratio. Radiation patterns with the y-direction misalignment are simulated as shown in Fig. 16. The y-direction

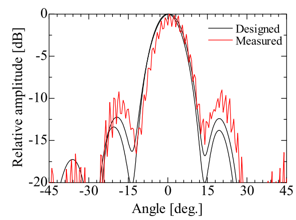

(a1)

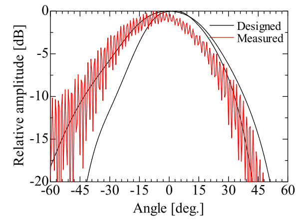

(a2)

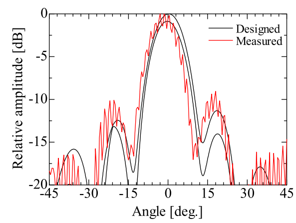

(b1)

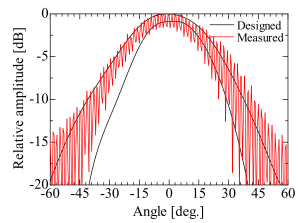

(b2)

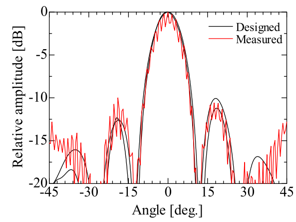

(c1)

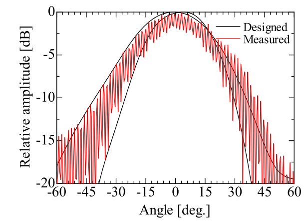

(c2)

FIGURE 15. Measured spinning linear patterns of (a1), (a2) $\phi = 0$ and 90° at 59.5 GHz, (b1), (b2) $\phi = 0$ and 90° at 60.5 GHz, (c1), (c2) $\phi = 0$ and 90° at 61.5 GHz.

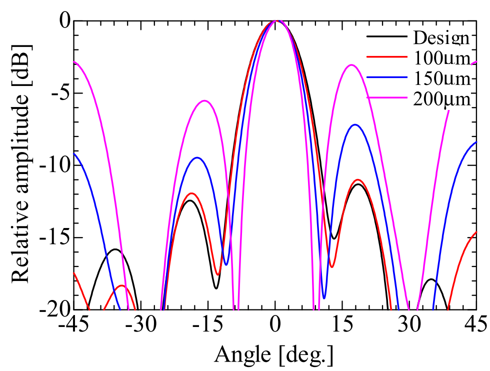

(a)

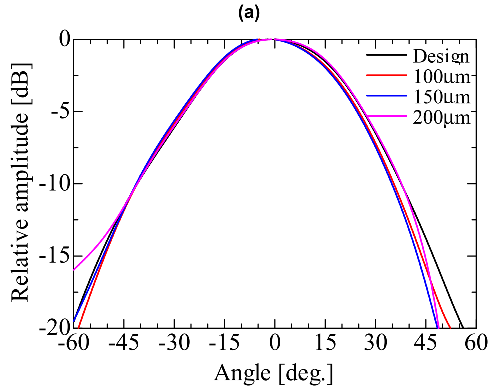

(b)

FIGURE 16. Radiation pattern at 60.5 GHz by y-direction misalignment (a) $\phi = 0$ and (b) 90°.

misalignment results in higher side lobe levels in the $\varphi = 0°$ plane whereas the effect on the 90° plane is negligible. This

TABLE 3. Comparison of circular polarized array antenna at 20-GHz and above.

Ref.	Freq. (GHz)	Element	Additional mechanical component	Feed	Fabrication technology	Number of dielectric layers	Number of metal layers	Number of elements	Antenna area (λ^2)	Axial ratio (dB)	Gain (dBi)	Effi-ciency* (%)
[9]	20.45	Dipole	Foam spacer	Hollow WG	Metal processing & PCB	NA	NA	12×12	78.6	0.95	27.9	62.5
[14]	28	Dipole	Air spacer	SIW	PCB & screwing	2	3	4×4	3.8	0.9	15.5	74.1
[12]	60	Elliptical patch	Reflector	MSL	Metal processing & PCB	1	2	4×2	4.3	1.2	15.6	67.5
[11]	60	Wide strip	None	SIW	LTCC	20	8	4×4	9.3	3.1	15	27.2
[19]	60	Helical	None	Strip-line	LTCC	20	11	4×4	4.0	1	15	62.8
[18]	60	Double spiral	None	SIW	PCB	3	6	4×4	10.9	1.2	18.5	51.8
[16]	60	ME-dipole	None	SIW	PCB	3	6	8×8	41.9	1.5	26	75.5
[17]	28	ME-dipole	None	Strip-line	PCB	3	4	4×4	5.0	2	18	72.0
[15]	37.5	Stacked curl	None	SIW	PCB	4	6	8×8	25.0	2.6	22.4	55.2
This work	61.5	Dipole	None	SIW	PCB	2	4	8×2	5.1	2.1	15.6	57.2

* Efficiency is calculated as $G/G\text{max}$ where G is the gain and Gmax is the maximum gain $4\pi A/\lambda^2$ where A is the antenna area and λ is the free space wavelength.

allows the conclusion that the measured higher side lobe levels result from the y-direction misalignment.

Table 3 details the designed antenna with previously published CP array antennas at 20-GHz and higher bands as shown in Table 3. The antennas [9], [14], and [12] require additional mechanical components decreasing ease of mass production. The other antennas in Table 3 are fabricated by LTCC or PCB, which are suitable for mass production. For mass production, the number of dielectric and metal layers should be the smallest possible. The proposed antenna realized the minimum number of dielectric layers with a comparable axial ratio, gain, and efficiency.

V. CONCLUSIONS

This paper presents an 8×2-element 60-GHz band circularly polarized post-wall waveguide slot array antenna loaded with dipoles. The antenna is composed of a feeding part, a radiating part, and a polarization conversion part. The integration of the feeding part and the radiating part into a single dielectric enables reduction of the total number of dielectric layers. The measured results show a 2.1-dB axial ratio, 15.6-dBi gain, and 57.2% efficiency at 61.5 GHz. The antenna consists of two dielectric and four metal layers and is fabricated by PCB. The number of dielectric layers is the minimum among the published investigations and suitable for mass production.

ACKNOWLEDGMENT

The authors wish to thank Drs. J. Iwasaki and K. Akiyama of Sony Semiconductor Solutions Corporation for their support.

REFERENCES

[1] *Part 11: Wireless LAN Medium Access Control (MAC) and Physical Layer (PHY) Specifications, Amendment 3: Enhancements for Very High Throughput in the 60 GHz Band*, IEEE Standard 802.11ad, Dec. 2012.

[2] T. S. Rappaport, S. Sun, R. Mayzus, H. Zhao, Y. Azar, K. Wang, G. N. Wong, J. K. Schulz, M. Samimi, and F. Gutierrez, "Millimeter wave mobile communications for 5G cellular: It will work!" *IEEE Access*, vol. 1, pp. 335–349, 2013.

[3] M. Zhang, K. Toyosaki, J. Hirokawa, M. Ando, T. Taniguchi, and M. Noda, "A 60-GHz band compact-range gigabit wireless access system using large array antennas," *IEEE Trans. Antennas Propag.*, vol. 63, no. 8, pp. 3432–3440, Aug. 2015.

[4] J. Huang, "A Ka-band circularly polarized high-gain microstrip array antenna," *IEEE Trans. Antennas Propag.*, vol. 43, no. 1, pp. 113–116, Jan. 1995.

[5] J. Hirokawa and M. Ando, "Single-layer feed waveguide consisting of posts for plane TEM wave excitation in parallel plates," *IEEE Trans. Antennas Propag.*, vol. 46, no. 5, pp. 625–630, May 1998.

[6] D. Deslandes and K. Wu, "Integrated microstrip and rectangular waveguide in planar form," *IEEE Microw. Wireless Compon. Lett.*, vol. 11, no. 2, pp. 68–70, Feb. 2001.

[7] R. Głogowski, C. Peixeiro, J. R. Mosig, and J.-F. Zürcher, "Broadband Ka-band rectangular waveguide to substrate integrated waveguide transition," *Electron. Lett.*, vol. 49, no. 9, pp. 602–604, Apr. 2013.

[8] K.-S. Min, J. Hirokawa, K. Sakurai, M. Ando, and N. Goto, "Single-layer dipole array for linear-to-circular polarisation conversion of slotted waveguide array," *IEE Proc. Microw. Antennas Propag.*, vol. 143, no. 3, pp. 211–216, 1996.

[9] M. Ferrando-Rocher, J. I. Herranz-Herruzo, A. Valero-Nogueira, and V. M. Rodrigo, "Circularly polarized slotted waveguide array with improved axial ratio performance," *IEEE Trans. Antennas Propag.*, vol. 64, no. 9, pp. 4144–4148, Sep. 2016.

[10] Y. Miura, J. Hirokawa, M. Ando, K. Igarashi, and G. Yoshida, "A high-efficiency circularly-polarized aperture array antenna with a corporate-feed circuit in the 60 GHz band," *IEICE Trans. Electron.*, vol. E94-C, no. 10, pp. 1618–1625, Oct. 2011.

[11] Y. Li, Z. N. Chen, X. Qing, Z. Zhang, J. Xu, and Z. Feng, "Axial ratio bandwidth enhancement of 60-GHz substrate integrated waveguide-fed circularly polarized LTCC antenna array," *IEEE Trans. Antennas Propag.*, vol. 60, no. 10, pp. 4619–4626, Oct. 2012.

[12] A. R. Weily and Y. J. Guo, "Circularly polarized ellipse-loaded circular slot array for millimeter-wave WPAN applications," *IEEE Trans. Antennas Propag.*, vol. 57, no. 10, pp. 2862–2870, Oct. 2009.
[13] W. Han, F. Yang, R. Long, L. Zhou, and F. Yan, "Single-fed low-profile high-gain circularly polarized slotted cavity antenna using a high-order mode," *IEEE Antennas Wireless Propag. Lett.*, vol. 15, pp. 110–113, 2016.
[14] M. Asaadi and A. Sebak, "High-gain low-profile circularly polarized slotted siw cavity antenna for MMW applications," *IEEE IEEE Antennas Wireless Propag. Lett.*, vol. 16, pp. 752–755, 2017.
[15] Q. Wu, J. Hirokawa, J. Yin, C. Yu, H. Wang, and W. Hong, "Millimeter-wave planar broadband circularly polarized antenna array using stacked curl elements," *IEEE Trans. Antennas Propag.*, vol. 65, no. 12, pp. 7052–7062, Dec. 2017.
[16] Y. Li and K.-M. Luk, "A 60-GHz wideband circularly polarized aperture-coupled magneto-electric dipole antenna array," *IEEE Trans. Antennas Propag.*, vol. 64, no. 4, pp. 1325–1333, Apr. 2016.
[17] J. Wu, Y. J. Cheng, and Y. Fan, "Millimeter-wave wideband high-efficiency circularly polarized planar array antenna," *IEEE Trans. Antennas Propag.*, vol. 64, no. 2, pp. 535–542, Feb. 2016.
[18] Q. Zhu, K.-B. Ng, and C. H. Chan, "Printed circularly polarized spiral antenna array for millimeter-wave applications," *IEEE Trans. Antennas Propag.*, vol. 65, no. 2, pp. 636–643, Feb. 2017.
[19] C. Liu, Y.-X. Guo, X. Bao, and S.-Q. Xiao, "60-GHz LTCC integrated circularly polarized helical antenna array," *IEEE Trans. Antennas Propag.*, vol. 60, no. 3, pp. 1329–1335, Mar. 2012.
[20] W.-W. Yang, W.-J. Sun, H. Tang, and J.-X. Chen, "Design of a circularly polarized dielectric resonator antenna with wide bandwidth and low axial ratio values," *IEEE Trans. Antennas Propag.*, vol. 67, no. 3, pp. 1963–1968, Mar. 2019.
[21] H. Yee, "Impedance of a narrow longitudinal shunt slot in a slotted waveguide array," *IEEE Trans. Antennas Propag.*, vol. 22, no. 4, pp. 589–592, Jul. 1974.
[22] Y. T. Lo and S. W. Lee, *Antenna Handbook*. New York, NY, USA: Van Nostrand Reinhold, 1988, Secs.12-4–12-6.
[23] L. Yan, W. Hong, K. Wu, and T. J. Cui, "Investigations on the propagation characteristics of the substrate integrated waveguide based on the method of lines," *IEE Proc.-Microw., Antennas Propag.*, vol. 152, no. 1, pp. 35–42, Feb. 2005.
[24] T. Kai, "Feed through an aperture to a post-wall waveguide with step structure," *IEICE Trans. Commun.*, vol. E88-B, no. 3, pp. 1298–1302, Mar. 2005.
[25] Y. Li and K.-M. Luk, "Low-cost high-gain and broadband substrate-integrated-waveguide-fed patch antenna array for 60-GHz band," *IEEE Trans. Antennas Propag.*, vol. 62, no. 11, pp. 5531–5538, Nov. 2014.
[26] Y. J. Cheng, K. Wu, and W. Hong, "Power handling capability of substrate integrated waveguide interconnects and related transmission line systems," *IEEE Trans. Adv. Packag.*, vol. 31, no. 4, pp. 900–909, Nov. 2008.
[27] K. Fukazawa, J. Hirokawa, M. Ando, and N. Goto, "Two way power divider for partially parallel feed in single-layer slotted waveguide arrays," *IEICE Trans. Commun.*, vol. E81-B, no. 6, pp. 1248–1254, Jun. 1998.
[28] B. Pyne, P. Akbar, H. Saito, M. Zhang, J. Hirokawa, and M. Ando, "Design of a center-feed waveguide feeder for wideband rectangular parallel-plate slot-array antenna on-board space-borne X-band SAR system," in *Proc. 46th Eur. Microw. Conf. (EuMC)*, London, U.K., Oct. 2016, pp. 1533–1536.
[29] *IEEE Standard Definitions of Terms for Antennas*, IEEE Standard 145-2013.
[30] W. L. Stutzman, *Polarization in Electromagnetic Systems*, 2nd ed. London, U.K.: Artech House, 2018.

TAKASHI TOMURA (Member, IEEE) received the B.S., M.S., and D.E. degrees in electrical and electronic engineering from the Tokyo Institute of Technology, Tokyo, Japan, in 2008, 2011, and 2014, respectively. He was a Research Fellow of the Japan Society for the Promotion of Science (JSPS), in 2013. From 2014 to 2017, he worked at Mitsubishi Electric Corporation, Tokyo, and was engaged in research and development of aperture antennas for satellite communications and radar systems. From 2017 to 2019, he was a specially appointed Assistant Professor with the Tokyo Institute of Technology, Tokyo, where he is currently an Assistant Professor. His research interests include electromagnetic analysis, aperture antennas, and planar waveguide slot array antennas.

Dr. Tomura is a member of the IEICE. He received the Best Student Award from Ericsson Japan, in 2012, the IEEE AP-S Tokyo Chapter Young Engineer Award, in 2015, and the Young Researcher Award from IEICE Technical Committee on Antennas and Propagation, in 2018.

YUTA SAITO received the B.S. and M.S. degrees in electrical and electronic engineering from the Tokyo Institute of Technology, in 2017 and 2019, respectively. He joined Panasonic Corporation, in 2019, where he was engaged in mobile device design.

JIRO HIROKAWA (Fellow, IEEE) received the B.S., M.S., and D.E. degrees in electrical and electronic engineering from the Tokyo Institute of Technology (Tokyo Tech), Tokyo, Japan, in 1988, 1990, and 1994, respectively.

He was a Research Associate, from 1990 to 1996, and an Associate Professor, from 1996 to 2015, with the Tokyo Tech, where he is currently a Professor. He was with the Antenna Group, Chalmers University of Technology, Gothenburg, Sweden, as a Postdoctoral Fellow, from 1994 to 1995. His research area has been in slotted waveguide array antennas and millimeter-wave antennas. He is a Fellow of IEICE. He received the IEEE AP-S Tokyo Chapter Young Engineer Award, in 1991, Young Engineer Award from IEICE, in 1996, Tokyo Tech Award for Challenging Research, in 2003, Young Scientists' Prize from the Minister of Education, Culture, Sports, Science, and Technology, Japan, in 2005, Best Paper Award, in 2007, Best Letter Award from the IEICE Communications Society, in 2009, and the IEICE Best Paper Award, in 2016 and 2018.